

# EnergyDiff: Universal Time-Series Energy Data Generation using Diffusion Models

Nan Lin, *Student Member, IEEE*, Peter Palensky, *Senior Member, IEEE*,  
Pedro P. Vergara, *Senior Member, IEEE*

**Abstract**—High-resolution time series data are crucial for operation and planning in energy systems such as electrical power systems and heating systems. However, due to data collection costs and privacy concerns, such data is often unavailable or insufficient for downstream tasks. Data synthesis is a potential solution for this data scarcity. With the recent development of generative AI, we propose *EnergyDiff*, a universal data generation framework for energy time series data. *EnergyDiff* builds on state-of-the-art denoising diffusion probabilistic models, utilizing a proposed denoising network dedicated to high-resolution time series data and introducing a novel Marginal Calibration technique. Our extensive experimental results demonstrate that *EnergyDiff* achieves significant improvement in capturing temporal dependencies and marginal distributions compared to baselines, particularly at the 1-minute resolution. Additionally, *EnergyDiff* consistently generates high-quality time series data across diverse energy domains, time resolutions, and at both customer and transformer levels with reduced computational need.

**Index Terms**—Generative models, load profile, data generation, time-series data.

## I. INTRODUCTION

THE rapid increase in the integration of renewable energy sources into energy systems has resulted in unprecedented volatility in energy generation. Additionally, the electrification of the energy systems has drastically altered energy consumption behaviors. Together, these factors pose significant challenges to energy systems' economical and safe operation and planning. To develop effective operation and planning solutions, energy system operators require accurate energy generation and consumption profiles [1], necessitating the collection of large amounts of high-resolution energy time series data. However, collecting such data is challenging due to privacy and cost concerns. Therefore, the need for algorithms that generate realistic energy time series data is crucial.

Conventional methods, such as Gaussian Mixture Models (GMMs) and t-Copula [2], [3] model, have been widely used for data generation due to their simplicity and historical effectiveness. In particular, t-Copula has the unique advantage of fitting the marginal distributions precisely, which is suitable for representing high-consumption or high-generation scenarios. However, these models struggle to capture the complex de-

pendencies inherent in high-resolution energy data, leading to sub-optimal performance in representing real-world scenarios.

Deep generative models offer more advanced solutions by capturing the intricate temporal patterns within the data. Examples are Generative Adversarial Networks (GANs) [4], [5], Variational Auto-encoders (VAEs) [6], and flow-based models [7]. Despite their strength, data generated by VAEs face challenges in maintaining high-resolution details; GANs suffer from mode collapse and training instability [8], [9]. Despite flow-based models having gained success in recent years [7], they intrinsically require an invertible neural network structure, limiting its expressing power. More importantly, little effort has been made to generate high-resolution time series data, i.e., 1-minute resolution or higher. For example, a daily electricity consumption profile has 1440 steps at the 1-minute resolution. This poses a great challenge to any generative models. Even fitting a simple Gaussian model with a full covariance matrix to such data would result in more than a million parameters. High-resolution data also leads to numerical instability for models like t-Copula as their fitting processes require the inversion of a large  $1440 \times 1440$  covariance matrix for every fitting step.

Denoising diffusion probabilistic models (DDPMs) are newly emerged deep generative models, which are easy to train and exhibit state-of-the-art data generation quality and diversity [10], [11], overcoming the disadvantages of previous deep generative models. These advantages make DDPM a natural candidate for a universal generative energy time series data model. Nevertheless, the state-of-the-art DDPM [12] was designed for image generation and faces several challenges when applied to energy time series generation. The first challenge is how to deal with high-resolution data, such as 1-minute data, as the computation complexity grows rapidly with the time series length due to the Transformer network architecture [13]. The second challenge is the inaccurate approximation of the marginal distributions. In the image field, the marginal distribution is the brightness distribution of pixels, which need not be extremely precise. However, in the energy field, the marginal distributions are important for characterizing the peak consumption and generation values. Recently, DDPM has been adopted to model electricity load profiles and electric vehicle (EV) charging scenarios [14]. The model proposed in [15] focuses more on a generative forecast problem, while [14] investigates a shorter time series, i.e., 720 steps, and circumvents the complexity issue by adopting a Long Short-Term Memory (LSTM) network architecture instead of a Transformer. Neither of these works has fully

This work used the Dutch national e-infrastructure with the support of the SURF Cooperative using grant no. EINF-6262. Nan Lin is funded by NWO Align4Energy Project NWA.1389.20.251.

Nan Lin, Peter Palensky, and Pedro P. Vergara are with the Intelligent Electrical Power Grids (IEPG) Group, Delft University of Technology, 2628 CD Delft, The Netherlands (e-mail:{N.Lin, P.P.VergaraBarrios, P.Palensky}@tudelft.nl).

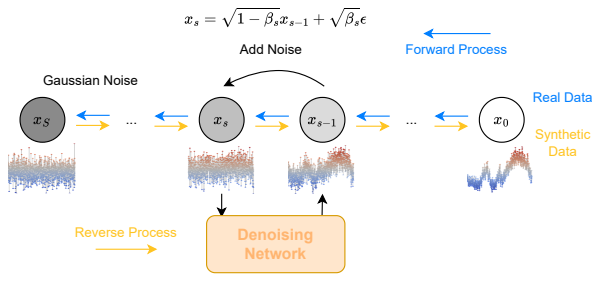


Fig. 1. In the forward process, noise is injected into the true data at gradually increasing levels; in the reverse process, the noise is iteratively removed from noisy data. In the proposed framework, we propose a denoising network using customized architecture (see Fig. 2) based on the Transformer network [13].

addressed the previous two challenges.

In this work, we propose *EnergyDiff*, a universal energy time series data generation framework based on DDPM, which is applicable across various energy domains, multiple time resolutions, and at both customer and electrical transformer levels. Furthermore, we propose a simple yet novel Marginal Calibration technique to combine the underlying dependency structure of DDPM and the empirical cumulative distribution functions (CDFs) of training samples, yielding almost exact marginal distributions on any model. Our contributions are summarized as follows.

- We propose *EnergyDiff*, a DDPM-based framework that is dedicated to generating energy time-series data. The proposed *EnergyDiff* is 1) scalable across different time resolutions and 2) applicable to generate data at both the transformer level and customer (household) level.
- To overcome the limitations of standard DDPM of modeling high-resolution time series data, we propose to use a folding operation in DDPM that quintessentially enables us to generate high-resolution data such as 1 minute with less computation than without the operation.
- We propose a Marginal Calibration technique that calibrates the inaccurate DDPM marginal distributions while preserving the learned complex temporal dependency structure. The proposed technique allows us to use prior knowledge about the marginal distributions in deep generative models. The generated data show significant improvement in terms of Kullback-Leibler divergence, Wasserstein distance, and Kolmogorov–Smirnov statistic.

## II. DENOISING DIFFUSION PROBABILISTIC MODELS

In this section, we introduce both the general theoretical framework of DDPM and the practical procedure of training and generation with DDPM. First, we formulate the probabilistic model by constructing two Markov chains. Next, we derive a loss function from the probabilistic model that can be used for efficient training with stochastic gradient descent (SGD). Finally, we show step-by-step how to generate new samples with a trained DDPM. A simple demonstration of DDPM procedure is shown in Fig. 1.

### A. Time Series Probabilistic Model

Any univariate time series data of  $T$  steps can be seen as a random vector  $\mathbf{x} \in \mathbb{R}^T$ . We assume it follows an unknown joint distribution  $\mathbf{x} \sim p(\mathbf{x})$ . Specifically, in energy time series data generation,  $\mathbf{x}$  represents a one-day consumption or generation profile. Consequently, the value of  $T$  changes with the time resolution. For hourly resolution,  $T = 24$ , while for 1-minute resolution,  $T = 1440$ . This formulation can be extended to multivariate time series and inter-day time series. For a  $m$ -variable  $T$ -step series, we can simply formulate  $\mathbf{x}$  as  $\mathbf{x} \in \mathbb{R}^{m \times T}$ . If one wants to generate a multi-day time series, for example, a weekly profile of hourly resolution, simply set  $T = 7 \cdot 24$ . In this paper, we only consider univariate daily time series. However, our framework naturally extends to multivariate cross-day scenarios.

### B. Diffusion Probabilistic Model Formulation

Overall, the idea of DDPM is to gradually corrupt data and learn how to recover the corrupted data through step-by-step denoising. To be consistent with the DDPM literature, we define  $\mathbf{x}_0 \equiv \mathbf{x}$  and the dimensionality  $d \equiv T$ . The subscript 0 represents the diffusion step, which will be explained later. With  $\mathbf{x}_0$  following an unknown distribution  $\mathbf{x}_0 \sim p(\mathbf{x}_0)$ , DDPM establishes a parametric distribution  $p_\theta(\mathbf{x}_0)$  to approximate the true data distribution  $p(\mathbf{x}_0)$ . Note that  $\theta$  is an abstract collection of all the parameters of the approximate distribution instead of a single parameter. We explain the detailed formulation of  $p_\theta(\mathbf{x}_0)$  below.

First, we define a *forward process* that corrupts the data iteratively with Gaussian noise for steps  $s = 0, 1, \dots, S$ , as follows

$$q(\mathbf{x}_s | \mathbf{x}_{s-1}) := \mathcal{N}(\sqrt{1 - \beta_s} \mathbf{x}_{s-1}, \beta_s \mathbf{I}) \quad (1)$$

$$q(\mathbf{x}_{1:S} | \mathbf{x}_0) := \prod_{s=1}^T q(\mathbf{x}_s | \mathbf{x}_{s-1}), \quad (2)$$

where  $\mathbf{x}_0$  is our observed data, and  $\beta_s \in (0, 1)$  is the corruption strength for diffusion step  $s$ , which usually increases gradually with  $s$ .  $\beta_s$  is a small number so that we do not corrupt the data too fast. The design for  $\{\beta_s\}$  is referred to as *noise schedule* in the literature [10], [16]. Notably, given  $\mathbf{x}_0$ , we can jump directly to any diffusion step  $s > 0$  by:

$$q(\mathbf{x}_s | \mathbf{x}_0) = \mathcal{N}(\sqrt{\alpha_s} \mathbf{x}_0, (1 - \alpha_s) \mathbf{I}), \quad (3)$$

where  $\alpha_s := 1 - \beta_s$ ,  $\bar{\alpha}_s := \prod_{\tau=1}^s \alpha_\tau$ . Here  $\bar{\alpha}_s$  can be intuitively seen as the signal strength of  $\mathbf{x}_s$ . Because  $\beta_s$  is between 0 and 1,  $\bar{\alpha}_s$  monotonically decreases. Consequently, when the final step  $S$  is large enough, the data will be almost completely corrupted; i.e.,  $q(\mathbf{x}_S | \mathbf{x}_0) \approx q(\mathbf{x}_S) = \mathcal{N}(\mathbf{0}, \mathbf{I})$ . In other words, we completely undermine the data with standard Gaussian noise at the last step of the forward process  $S$ .

Now, we shift our focus to the *reverse process*, where we start with the fully corrupted data  $\mathbf{x}_S$  to get the original data  $\mathbf{x}_0$ . If we know the exact denoising distribution  $q(\mathbf{x}_{s-1} | \mathbf{x}_s)$ , for any  $s$ , we can sample  $\mathbf{x}_S \sim \mathcal{N}(\mathbf{0}, \mathbf{I})$  and go through the forward process in reverse direction to obtain  $\mathbf{x}_0$ . However,  $q(\mathbf{x}_{s-1} | \mathbf{x}_s)$  is not tractable. Naturally, we can approximate it with the following distribution parameterized by  $\theta$

$$p_\theta(\mathbf{x}_{s-1} | \mathbf{x}_s) := \mathcal{N}(\boldsymbol{\mu}_\theta(\mathbf{x}_s, s), \boldsymbol{\Sigma}_\theta(\mathbf{x}_s, s)). \quad (4)$$

The two functions  $\mu_\theta$  and  $\Sigma_\theta$  tell us how we can denoise  $\mathbf{x}_s$  to get the less noisy  $\mathbf{x}_{s-1}$ .

The exact and approximate joint distribution over  $\mathbf{x}_{0:S}$  are

$$q(\mathbf{x}_{0:S}) = p(\mathbf{x}_0) \prod_{s=1}^T q(\mathbf{x}_s | \mathbf{x}_{s-1}) \quad (5)$$

$$p_\theta(\mathbf{x}_{0:S}) = q(\mathbf{x}_S) \prod_{s=1}^S p_\theta(\mathbf{x}_{s-1} | \mathbf{x}_s). \quad (6)$$

### C. Training DDPM

DDPM consists of the forward and reverse processes. The forward process is simply corrupting data and is only a means to an end. Generating data requires only the reverse process, which reduces to evaluating two parametric functions,  $\mu_\theta$  and  $\Sigma_\theta$ . During the training process, we find the parametric functions  $\mu_\theta$  and  $\Sigma_\theta$  by minimizing a loss function evaluated on a set of training samples  $\{\mathbf{x}_0^{(i)}\}_{i=1}^N$ .

1) *Loss Function*: To minimize the discrepancy between the true distribution  $p(\mathbf{x}_0)$  and the approximate distribution  $p_\theta(\mathbf{x}_0)$ , we can minimize the negative evidence lower bound (ELBO)

$$\begin{aligned} \mathcal{L}_\theta &:= \mathbb{E}_{\mathbf{x}_{1:S} \sim q, \mathbf{x}_0 \sim p} \left[ -\log \frac{p_\theta(\mathbf{x}_{0:S})}{q(\mathbf{x}_{1:S} | \mathbf{x}_0)} \right] \quad (7) \\ &= \mathbb{E}_{\mathbf{x}_0 \sim p} [-\log p_\theta(\mathbf{x}_0) + D_{KL}(q(\mathbf{x}_{1:S} | \mathbf{x}_0) || p_\theta(\mathbf{x}_{1:S} | \mathbf{x}_0))] \\ &\geq \mathbb{E}_{\mathbf{x}_0 \sim p} [-\log p_\theta(\mathbf{x}_0)]. \end{aligned}$$

By optimizing  $\mathcal{L}_\theta$ , we jointly maximize the log likelihood of data on our model  $\log p_\theta(\mathbf{x}_0)$  and minimizes the approximation error between  $p_\theta$  and the true distribution  $p(\mathbf{x}_0)$ .

Essentially, the parametric functions we need to learn are  $\mu_\theta : \mathbb{R}^d \times \mathbb{Z}_{0+} \rightarrow \mathbb{R}^d$  and  $\Sigma_\theta : \mathbb{R}^d \times \mathbb{Z}_{0+} \rightarrow \mathbb{S}_+^d$ , where  $\mathbb{S}_+^d$  is the set of all  $d \times d$  positive semi-definite matrices. Naturally, we can use neural networks to parameterize these two functions. Since these two functions essentially serve the purpose of partially removing the noise in  $\mathbf{x}_s$  to recover  $\mathbf{x}_{s-1}$ , we will refer to them as the *denoising networks*. The powerful capacity of neural networks can therefore enable us to learn complex joint distributions. As [10] suggests, the variance function  $\Sigma_\theta$  can be fixed to  $\Sigma_\theta = \beta_s \mathbf{I}$  with little to no performance drop. Furthermore, for efficient training with SGD, we can derive a loss function from (7) as

$$\hat{\mathcal{L}}_\theta^{\text{simple}} = \frac{1}{B} \sum_{i=1}^B \frac{1}{2\tilde{\beta}_{s_i}} \|\tilde{\mu}_{s_i}(\mathbf{x}_{s_i}^{(i)}, \mathbf{x}_0^{(i)}) - \mu_\theta(\mathbf{x}_{s_i}^{(i)}, s_i)\|_2^2, \quad (8)$$

$$\tilde{\mu}_s(\mathbf{x}_s, \mathbf{x}_0) = \frac{\sqrt{\alpha_{s-1}} \beta_s}{1 - \bar{\alpha}_s} \mathbf{x}_0 + \frac{\sqrt{\alpha_s} (1 - \bar{\alpha}_s)}{1 - \bar{\alpha}_s} \mathbf{x}_s \quad (9)$$

where  $\{\mathbf{x}_0^{(i)}\}_{i=1}^B$  are a batch of  $B$  samples drawn from the complete dataset  $\{\mathbf{x}_0^{(i)}\}_{i=1}^N$ , and each  $s_i$  is uniformly and independently drawn from  $\{1, \dots, S\}$ . Taking the gradient  $\nabla_\theta \hat{\mathcal{L}}_\theta^{\text{simple}}$  enables us to perform SGD.

2) *Training Procedures*: Despite the complex construction of DDPM, the training procedure is simple. We summarize it in Algorithm 1.

### D. Generation Procedure

Once the training is done and parameters  $\theta$  are obtained, we can generate new data through the *reverse process*. As

---

### Algorithm 1 Training DDPM

---

**Require:** Dataset  $\{\mathbf{x}_0^{(i)}\}_{i=1}^N$ , initialized  $\mu_\theta$ , learning rate  $\eta$ , noise schedule  $\{\beta_s, \alpha_s, \bar{\alpha}_s\}$   
**while** not converged **do**  
    Draw samples  $\{\mathbf{x}_0^{(i)}\}_{i=1}^B$  from the dataset  
    Sample diffusion step  $\{s_i | s_i \sim \mathcal{U}\{1, S\}\}$   
    Forward  $0 \rightarrow s_i$ :  $\mathbf{x}_{s_i}^{(i)} = \sqrt{\bar{\alpha}_{s_i}} \mathbf{x}_0^{(i)} + \sqrt{1 - \bar{\alpha}_{s_i}} \epsilon_{s_i}$   
    Reverse  $s_i \rightarrow s_i - 1$ :  $\mu_\theta(\mathbf{x}_{s_i}^{(i)}, s_i)$   
     $\theta \leftarrow \theta + \eta \nabla_\theta \hat{\mathcal{L}}_\theta^{\text{simple}}(\mathbf{x}_{s_i}^{(i)}, \mathbf{x}_0^{(i)}, \mu_\theta(\mathbf{x}_{s_i}^{(i)}, s_i))$   
**end while**

---



---

### Algorithm 2 Sampling new data from DDPM

---

**Require:** trained  $\mu_\theta$ , noise schedule  $\{\beta_s, \alpha_s, \bar{\alpha}_s\}$   
Initialize  $s = S$   
Sample  $\mathbf{x}_S \sim \mathcal{N}(\mathbf{0}, \mathbf{I})$   
**while**  $s > 0$  **do**  
    Reverse: Calculate  $\hat{\mu}_{s-1} = \mu_\theta(\mathbf{x}_s, s)$   
    Sample  $\mathbf{x}_{s-1} \sim \mathcal{N}(\hat{\mu}_{s-1}, \tilde{\beta}_s \mathbf{I})$   
     $s \leftarrow s - 1$   
**end while**  
**return**  $\mathbf{x}_0$

---

summarized in Algorithm 2, we start with sampling noise  $\mathbf{x}_S$  from a standard normal distribution. Following that, we recursively denoise from  $\mathbf{x}_s$  to  $\mathbf{x}_{s-1}$  for  $S$  times with the help of denoising distribution  $p_\theta(\mathbf{x}_{s-1} | \mathbf{x}_s)$ . Finally, we achieve clean sample  $\mathbf{x}_0$  that approximately follows the true data distribution  $p(\mathbf{x}_0)$ .

## III. ENERGYDIFF ARCHITECTURE

DDPM is a powerful probabilistic model that can approximate complex distributions. However, there is a notable lack of effort in developing a robust and universally applicable DDPM capable of generating high-resolution energy time series data of various energy domains. There are several challenges in modeling energy time series data by commonly adopted GMM and the standard DDPM. First, the temporal dependencies of energy data vary significantly across different domains and are often complex. Second, the computation and memory complexity can grow dramatically as the time resolution increases. For example, a daily electricity consumption profile with a 1-minute resolution yields a 1440-dimensional vector. This means even a simple Gaussian model with a full covariance matrix would have over a million parameters. Third, neural network-based methods can usually learn complex dependency structures well, but the learned marginal distributions are far less accurate than the empirical cumulative distribution function (ECDF), which is easy to estimate.

We address all of these challenges in our proposed *EnergyDiff* framework, which is dedicated to energy time series data generation. The forward process follows the exact same paradigm as the original DDPM, while the reverse process consists of our tailored denoising network. We also propose an additional Marginal Calibration step upon the completion of the reverse process, which compensates for

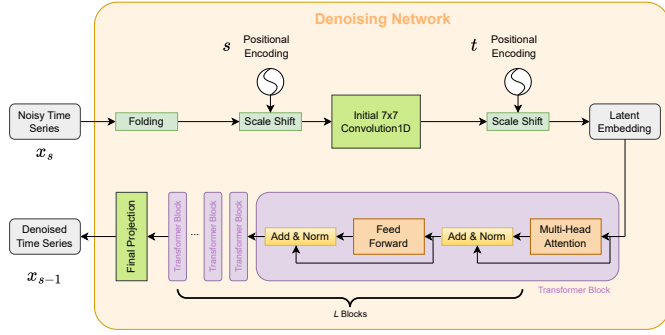


Fig. 2. Denoising Network Architecture. The network predicts denoised  $\mathbf{x}_{s-1}$  based on noisy  $\mathbf{x}_s$ , letting us advance one step in the *reverse process*. After the Folding, Initial Convolution, and Positional Encoding blocks, the Transformer blocks serve a central role in denoising data by learning its temporal dependency.

the inaccuracy of the DDPM on marginal distributions. The complete framework is demonstrated in Fig. 1.

### A. Tailored Reverse Process

Learning the temporal dependency structure is central in generating the energy time series data. To achieve this, we propose the neural network architecture shown in Fig. 2. The proposed architecture exploits Transformer<sup>1</sup> networks' capacity for processing sequential data (such as time series data) [13]. As we will show in Section V, such a design allows *EnergyDiff* to learn complex temporal patterns across different energy domains. Besides the Transformer blocks, the proposed architecture comprises a Folding block, a two-level Positional Encoding block, an Initial Convolution block, and a Final Projection block.

1) *Folding*: Transformer is a powerful model that captures complex temporal patterns. However, its memory and computation complexity is quadratic to the time series length [13]. This means whenever time resolution is doubled, we will have four times the computation and memory cost. Sequence length also heavily influences time complexity because of massive memory read/write operations. Therefore, to deal with high-resolution time series, e.g., 1 minute, we propose to use a folding operation as the first step. For a multivariate time series data  $\mathbf{x}_0 \in \mathbb{R}^{d \times T}$ , we fold every consecutive  $r$  steps into the channel dimension. This can be represented as

$$\tilde{\mathbf{x}}_0 \in \mathbb{R}^{dr \times \frac{T}{r}} \leftarrow \mathbf{x}_0 \in \mathbb{R}^{d \times T}. \quad (10)$$

For long sequences, the computation of Transformers is intensive mostly because of the Attention operation. Specifically, the memory complexity of Attention for sequence length  $L$  is nearly  $\mathcal{O}(L^2)$ . Such a folding operation would reduce the complexity of Transformer operations by  $r^2$  times. Fig. 3 shows an example of this operation.

2) *Positional Encoding*: Before passing data to the Transformer blocks, we need to embed positional information into the data. There are two types of *positions* we need to inform. Generally, for a multivariate sequence at the  $s$ -th step in

<sup>1</sup>We only refer to the neural network model proposed [13] as Transformer in this section.

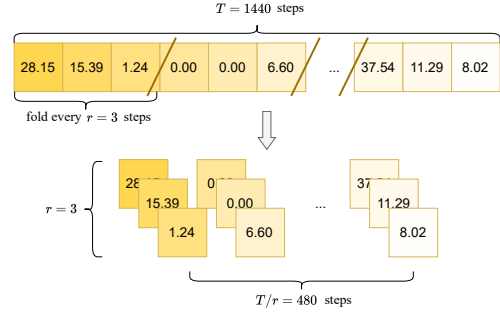


Fig. 3. A long univariate time series of 1440 steps is folded into a shorter 3-variable (or 3-channel) multivariate time series of 480 steps, with a folding factor  $r = 3$ .

the diffusion process,  $\mathbf{x}_s \in \mathbb{R}^{d \times T}$ . The first *position* is  $s \in \{0, 1, \dots, S\}$ , which is implicitly associated with the noise level; the second *position* is  $t \in \{0, 1, \dots, T-1\}$ , the position in the time series. We embed each of them separately through the same mechanism called positional encoding [13] and a learned scale and shift.

$$\text{PE}_{2i}(pos, d) = \sin\left(\frac{pos}{10000^{2i/d}}\right) \quad (11)$$

$$\text{PE}_{2i+1}(pos, d) = \cos\left(\frac{pos}{10000^{2i/d}}\right), \quad (12)$$

where  $\text{PE}(\cdot, d) : \mathbb{N} \rightarrow [-1, 1]^d$  is a vector function that maps a position  $pos$  to a  $d$ -dimensional vector for any given  $d$ . Each one element of the  $d$ -dimensional output has different sensitivities to the change of  $pos$ . Next we use two fully connected layers to scale and shift  $\mathbf{x}_s$ . For *diffusion step encoding*, we have

$$\boldsymbol{\sigma}(s) = W_2^{\text{scale}} \text{SiLU}(W_1 \text{PE}(s, d) + \mathbf{b}_1) + \mathbf{b}_2^{\text{scale}} \quad (13)$$

$$\boldsymbol{\delta}(s) = W_2^{\text{shift}} \text{SiLU}(W_1 \text{PE}(s, d) + \mathbf{b}_1) + \mathbf{b}_2^{\text{shift}}, \quad (14)$$

where  $W$  (matrix) and  $\mathbf{b}$  (vector) are weights and biases that will be learnt during training, and SiLU is the Sigmoid Linear Unit activation function proposed by [17]. With  $\boldsymbol{\sigma}(s) \in \mathbb{R}^d$  and  $\boldsymbol{\delta}(s) \in \mathbb{R}^d$ , we scale and shift  $\mathbf{x}_{s,t}$  by

$$\mathbf{x}_{s,t} \leftarrow (1 + \boldsymbol{\sigma}(s)) \odot \mathbf{x}_{s,t} + \boldsymbol{\delta}(s), \quad (15)$$

where  $\odot$  is the Hadamard (element-wise) product. The scale and shift are only determined by  $s$  and stay the same for  $\forall t$  given the same  $s$ . We use  $1 + \boldsymbol{\sigma}(s)$  instead of  $\boldsymbol{\sigma}(s)$  and initialize  $\boldsymbol{\sigma}$  and  $\boldsymbol{\delta}$  with zero, as this showed capabilities of stabilizing the training.

Additionally, another Positional Encoding is added for *time step*  $t$ , as shown in Fig. 2. This Positional Encoding is placed after Initial Convolution and before the Transformer blocks. After the Initial Convolution, we have sequence  $\mathbf{x}'_s \in \mathbb{R}^{d' \times T}$ . We use the same sinusoidal positional encoding with a different dimensionality  $\text{PE}(t, d')$  and another two fully connected layers applying scale and shift on  $\mathbf{x}'_{s,t}$ .

$$\boldsymbol{\sigma}'(t) = W_2'^{\text{scale}} \text{SiLU}(W_1' \text{PE}(t, d') + \mathbf{b}'_1) + \mathbf{b}'_2^{\text{scale}} \quad (16)$$

$$\boldsymbol{\delta}'(t) = W_2'^{\text{shift}} \text{SiLU}(W_1' \text{PE}(t, d') + \mathbf{b}'_1) + \mathbf{b}'_2^{\text{shift}}, \quad (17)$$

where the  $W$  matrices and  $\mathbf{b}$  vectors are also learnable parameters. Different from above, we scale and shift  $\mathbf{x}'_{s,t}$  by

$$\mathbf{x}'_{s,t} \leftarrow (1 + \boldsymbol{\sigma}'(t)) \odot \mathbf{x}'_{s,t} + \boldsymbol{\delta}'(t). \quad (18)$$

The scale and shift is only determined by  $t$  and stay the same for  $\forall s$ .

3) *Initial Convolution*: After folding and positional encoding for  $s$ , we employ a large kernel convolution, which is proved useful as an initial feature extractor [18]. We use the same convolution for  $\forall s$ .

$$\mathbf{x}'_{s,t} = \sum_{\tau=-k}^k W_{\tau}^{\text{init}} \mathbf{x}_{s,t-\tau} + \mathbf{b}^{\text{init}}, \quad (19)$$

where  $2k+1$  is the convolution kernel size;  $W_{\tau}^{\text{init}} \in \mathbb{R}^{d' \times d}$  and  $\mathbf{b}^{\text{init}} \in \mathbb{R}^{d'}$  are the learnable weight matrices and bias. Since  $t_{\min} = 0$ , we use a circular padding for  $\mathbf{x}_{s,t-1}, \dots, \mathbf{x}_{s,t-k}$ .

4) *Transformer Blocks*: The transformer blocks are our main tool for learning temporal dependency. Since our task is denoising, we do not need the *encoder-decoder* structure in [13]. Instead, we only adopt the decoders. This has been proven to work effectively for image generation [12]. There are two main sub-blocks in a Transformer block, namely multi-head attention (MHA) and feed forward network (FFN). We use a total of  $L$  Transformer blocks. For block  $l$ , it takes the output of previous block  $\mathbf{x}_{s,t}^{(l-1)}$  as input and passes its output  $\mathbf{x}_{s,t}^{(l)}$  to the next block. The initial input is  $\mathbf{x}_{s,t}^{(0)} := \mathbf{x}'_{s,t}$ , with the final output being  $\mathbf{x}_{s,t}^{(L)}$ . We fix the dimensionality of the input and output such that

$$\text{Block}_l : \mathbf{x}_{s,t}^{(l-1)} \in \mathbb{R}^{d' \times T} \rightarrow \mathbf{x}_{s,t}^{(l)} \in \mathbb{R}^{d' \times T}, \quad \forall l \{1, \dots, L\}. \quad (20)$$

MHA is the core operation of Transformer. It extracts the temporal features by comparing the sequence at each time step with any other time step. An MHA has  $H$  heads; each head operates separately and is aggregated later. Using multiple heads allows the attention mechanism to focus on different attributes of the data. For head  $h$  in the  $l$ -th Transformer block, we first calculate

$$\mathbf{q}_{l,h} = W_{l,h}^q \mathbf{x}_{s,t}^{(l-1)} \quad (21)$$

$$\mathbf{k}_{l,h} = W_{l,h}^w \mathbf{x}_{s,t}^{(l-1)} \quad (22)$$

$$\mathbf{v}_{l,h} = W_{l,h}^v \mathbf{x}_{s,t}^{(l-1)}, \quad (23)$$

where  $W_{l,h}^q, W_{l,h}^w, W_{l,h}^v \in \mathbb{R}^{\frac{d'}{H} \times d'}$  are learnable matrices.  $\mathbf{q}_{l,h}, \mathbf{k}_{l,h}, \mathbf{v}_{l,h}$  are called queries, keys, and values respectively. For each of the  $T$  query, the idea is to calculate the similarity between the query and each of the  $T$  keys with dot product. After normalizing the dot product, we have a series of similarity weights that sum up to one. We then use these weights to perform a weighted average of the associated values.

$$\text{Attention}_h(\mathbf{q}_{l,h}, \mathbf{k}_{l,h}, \mathbf{v}_{l,h}) = \mathbf{v}_{l,h} \text{softmax}\left(\frac{\mathbf{k}_{l,h}^T \mathbf{q}_{l,h}}{\sqrt{d'/H}}\right) \quad (24)$$

$$\text{softmax}_{m,n}(\zeta) := \frac{e^{\zeta_{m,n}}}{\sum_{i=1}^M e^{\zeta_{i,n}}}, \quad \zeta \in \mathbb{R}^{M \times N}, \quad (25)$$

where the softmax function normalizes a matrix by the columns. The sum of any column of the softmax output is

always one. Each attention head operates independently and their outputs are concatenated to get the final output.

$$\begin{aligned} & \text{MHA}(\mathbf{x}_s^{(l-1)}) \\ &= \text{Concat}(\text{Attention}_1, \text{Attention}_2, \dots, \text{Attention}_H), \end{aligned} \quad (26)$$

where the output has the same shape as the input  $\mathbb{R}^{d' \times T}$ .

Following the MHA, we add a LayerNorm and a skip connection.

$$\tilde{\mathbf{x}}_{s,t}^{(l-1)} = \text{LayerNorm}(\mathbf{x}_{s,t}^{(l-1)}) + [\text{MHA}(\mathbf{x}_s^{(l-1)})]_t \quad (27)$$

$$\text{LayerNorm}(\mathbf{x}_{s,t}^{(l-1)}) = \frac{\mathbf{x}_{s,t}^{(l-1)} - \mathbb{E}[\mathbf{x}_{s,t}^{(l-1)}]}{\sqrt{\text{Var}[\mathbf{x}_{s,t}^{(l-1)}] + \epsilon}} \odot \boldsymbol{\gamma} + \boldsymbol{\beta}, \quad (28)$$

where LayerNorm normalizes  $\mathbf{x}_{s,t}^{(l-1)} \in \mathbb{R}^{d'}$  over the  $d'$  elements.  $\epsilon$  is a small number for numerical stability.  $\boldsymbol{\gamma}$  and  $\boldsymbol{\beta}$  are learnable  $\mathbb{R}^{d'}$  vectors.

Next, we pass  $\tilde{\mathbf{x}}_{s,t}^{(l-1)}$  to a two-layer feed forward (fully connected) network.

$$\text{FFN}(\tilde{\mathbf{x}}_{s,t}^{(l-1)}) = W_{l,2}^{\text{FF}} \text{SiLU}(W_{l,1}^{\text{FF}} \tilde{\mathbf{x}}_{s,t}^{(l-1)} + \mathbf{b}_{l,1}^{\text{FF}}) + \mathbf{b}_{l,2}^{\text{FF}}, \quad (29)$$

where the  $W$  matrices and  $b$  vectors are learnable weights and biases. Consequently, we get out final output of this layer with another LayerNorm and a skip connection.

$$\mathbf{x}_{s,t}^{(l)} = \text{LayerNorm}(\tilde{\mathbf{x}}_{s,t}^{(l-1)}) + \text{FFN}(\tilde{\mathbf{x}}_{s,t}^{(l-1)}) \quad (30)$$

5) *Final Projection*: After  $L$  blocks of Transformer, we perform an affine projection on concatenated  $\mathbf{x}_{s,t}^{(L)}$  and  $\mathbf{x}_{s,t}^{(0)}$ . This serves as a partial skip connection that helps with building deep networks.

$$\hat{\boldsymbol{\mu}}_{s-1,t} = W^{\circ} \text{Concat}(\mathbf{x}_{s,t}^{(0)}, \mathbf{x}_{s,t}^{(L)}) + \mathbf{b}^{\circ}, \quad (31)$$

where  $W^{\circ}$  and  $\mathbf{b}^{\circ}$  are learnt parameters.  $\hat{\boldsymbol{\mu}}_{s-1}$  is the estimated mean of denoising distribution  $p_{\theta}(\mathbf{x}_{s-1} | \mathbf{x}_s) = \mathcal{N}(\hat{\boldsymbol{\mu}}_{s-1}, \hat{\boldsymbol{\beta}}_s \mathbf{I})$ , and  $\theta$  is the collection of all of the learnable parameters above.

## B. Optimal Marginal Calibration

All joint distributions comprise two elements: the dependency structure and the marginal distributions. Estimating the dependency structure is generally challenging, whereas the marginal distributions can be straightforwardly and precisely estimated by methods such as ECDF or simple parametric 1D distributions when prior knowledge is available. Neural network-based models approximate these two elements simultaneously by minimizing the ELBO. In practice, the resulting marginal distributions can have significant discrepancies with the true marginal distributions. To address these inaccuracies, we propose a marginal calibration process utilizing optimal transport (OT) mapping. This calibration applies the minimal alterations, maintaining the original temporal dependency structure while aligning the variables with the accurate marginal distributions.

1) *Re-estimate Marginal Distribution*: First, we acquire a new estimate of the marginal distributions. In the most general case, we exploit the marginal ECDF, which is an unbiased and easily accessible estimate of the true marginal CDF. According to the Glivenko–Cantelli theorem, it converges almost surely to the true distribution. Practically, there is often prior knowledge about the marginal distribution of energy time series data. For example, the marginals of residential electrical energy consumption often follow a log-normal or gamma distribution [19]. In such cases, we can perform more accurate and statistically sound estimations by maximum likelihood or maximum a posteriori (MAP). Formally, to obtain ECDF of the real (training) data, we have

$$F_t^*(\nu) = \frac{1}{N} \sum_{i=1}^N \mathbf{1}_{x_{0,t} \leq \nu} (x_{0,t}^{(i)}) \quad (32)$$

$$\mathbf{1}_{x_{0,t} \leq \nu} (x_{0,t}^{(i)}) = \begin{cases} 1 & \text{if } x_{0,t}^{(i)} \leq \nu \\ 0 & \text{otherwise} \end{cases} \quad (33)$$

where  $x_{0,t}^{(i)}$  is the  $t$ -th time step of the  $i$ -th sample taken from the training set  $\{x_0^{(i)}\}_{i=1}^N$ .  $\mathbf{1}_{x_{0,t} \leq \nu}(x)$  is an indicator function that outputs 1 if the input is less than or equal to  $\nu$  and 0 otherwise.

Meanwhile, we also estimate the (inaccurate) marginal distributions of DDPM. After training our model, we first generate  $M$  synthetic samples  $\{\hat{x}_0^{(i)}\}_{i=1}^M$ . The ECDF of DDPM is therefore given by

$$F_t'(\nu) = \frac{1}{m} \sum_{i=1}^m \mathbf{1}_{\hat{x}_{0,t}^{(i)} \leq \nu}, \quad (34)$$

where  $\hat{x}_{0,t}^{(i)}$  is generated synthetic sample.

2) *Optimal Transport Calibration*: Next, we seek a way to replace the inaccurate marginal distributions  $F_t'$  with the more accurate ones  $F_t^*$ . We find this mapping  $g_t$  by solving the following optimization problem

$$\begin{aligned} \min_{g_t} \mathbb{E}_{\hat{x}_{0,t} \sim F_t'} [ \|\hat{x}_{0,t} - g_t(\hat{x}_{0,t})\|_2^2 ] \\ \text{s.t. } \forall \hat{x}_{0,t} \sim F_t', g_t(\hat{x}_{0,t}) \sim F_t. \end{aligned} \quad (35)$$

The constraints indicate that the mapping  $g_t$  must transform a random variable from the distribution  $F_t'$  into a random variable that conforms to the new distribution  $F_t$ . The objective implies that we seek a mapping  $g_t$  close to the identity mapping, as it minimizes  $\mathbb{E}_{\hat{x}_{0,t} \sim F_t'} [ \|\hat{x}_{0,t} - g_t(\hat{x}_{0,t})\|_2^2 ]$ .

This problem is also known as the OT problem. The exact solution is called OT mapping. In general, the OT problem is a complex functional problem. However, in the one-dimensional case, it is proved that a mapping is the OT mapping if and only if it monotonically increases and satisfies the constraint in (35). In our specific case, we notice that the function  $F_t^{*-1} \circ F_t'$  satisfies exactly these two conditions. Therefore, the exact OT mapping  $g_t^*$  is given by

$$g_t^*(\hat{x}_{0,t}) = F_t^{*-1}(F_t'(\hat{x}_{0,t})) \quad \forall t. \quad (36)$$

For any synthetic sample  $\hat{x}_0$  from DDPM, the calibration is done as

$$\hat{x}'_{0,t} \leftarrow F_t^{*-1}(F_t'(\hat{x}_{0,t})) \quad \forall t. \quad (37)$$

TABLE I  
OVERVIEW OF DATASETS IN CASE OF STUDY.

Name	Country	Type	Resolution	Level
WPuQ [21]	Germany	Heat Pump	1min~1h	Household
WPuQ [21]	Germany	Electricity	1min~1h	Substation
WPuQ [21]	Germany	PV	1min~1h	Household
LCL [20]	UK	Electricity	30min~1h	Household
CoSSMic [22]	Germany	Electricity	1min 1h	Household
CoSSMic [22]	Germany	PV	1min 1h	Household

## IV. CASE OF STUDY

### A. Datasets

We show *EnergyDiff*'s flexibility and capability of modeling high-dimensional data by selecting a diverse set of data sources across various energy domains, time resolutions, and at both customer household and transformer levels. We preprocess all datasets by splitting them into daily profiles, and we see these profiles as identical independent samples. Depending on the time resolution, the daily profile time series lengths range from 24 at a 1-hour resolution to 1440 at a 1-minute resolution. We categorize the datasets into three classes. First, residential electricity load profiles at the customer level. This type of data comes from the Low Carbon London (LCL) [20] project, WPuQ [21] project and CoSSMic [22] project. Second, residential household heat pump electricity consumption data from the WPuQ project. Third, transformer-level electricity consumption and PV generation data from the WPuQ project. We summarize the selected datasets in Table I.

### B. Evaluation Metrics

Because of the high-dimensional nature of time series data, it is difficult to apply conventional probability theory-based measures to examine the joint distribution divergence between the real and generated samples. Nonetheless, several metrics have been established to measure the quality of synthetic data. We will give a brief introduction to these metrics, while the details and equations can be found in [23].

1) *Gaussian Frechét Distance*: The Frechét distance (FD) was proposed and adapted to compare the similarity between two probability distributions. Despite the intractability of FD for high-dimensional joint distributions, an analytical solution exists between two multivariate Gaussian distributions. Therefore, we can generalize FD to Gaussian Frechét distance (GFD) to measure the similarity between any two multivariate joint distributions because it quantifies simultaneously the differences in the mean and covariance matrices.

2) *Maximum Mean Discrepancy (MMD)*: Maximum Mean Discrepancy is a kernel-based disparity measure. It embeds samples of arbitrary data space (e.g.,  $\mathbb{R}^d$ ) into a reproducing kernel Hilbert space (RKHS) and compares two distributions by the largest difference in expectations over their embeddings in the RKHS. MMD measures both the dependency structure and the marginal distribution through an implicit feature mapping via the kernels.

3) *Wasserstein Distance (WD)*: Wasserstein distance measures the minimum distance between two distributions with the optimal coupling. A coupling of  $\mathbf{x}$  and  $\mathbf{y}$  is a joint distribution over  $\text{Concat}(\mathbf{x}, \mathbf{y})$ , whose marginal distributions satisfies  $\int_{\mathbf{y}} c(\mathbf{x}, \mathbf{y}) = p_X(\mathbf{x})$  and  $\int_{\mathbf{x}} c(\mathbf{x}, \mathbf{y}) = p_Y(\mathbf{y})$ . Taking the

infimum suggests that the coupling  $c$  in Wasserstein distance seeks to connect  $x$  and  $y$  in the shortest path possible. In other words, WD measures the shortest distance between two distributions. However, it is generally intractable to find such coupling between two high-dimensional joint distributions. Therefore, we only compare the Wasserstein distance between their marginal distributions in the following section.

4) *Kullback-Leibler (KL) Divergence*: Unlike WD, KL divergence measures the discrepancy between two distributions from the perspective of the information theory. Unfortunately, calculating KL divergence between high-dimensional distributions is also generally not possible. Again, we will evaluate KL divergence between the marginal distributions.

5) *Kolmogorov-Smirnov (KS) Statistic*: The two-sample KS test is a procedure to check whether two underlying one-dimensional distributions differ. It exploits the KS statistic, defined as the largest difference between two CDFs across all  $x$ . Similarly, we will evaluate the KS statistic between the marginal distributions, as KS statistic is not tractable for high-dimensional joint distribution.

### C. Model Setup

Due to the versatility of our framework, we use the same setup for all experiments in this section. Specifically, we implement *EnergyDiff* in PyTorch. The Transformer blocks have  $L = 12$  layers and  $d' = 512$  neurons in each block. The number of neurons in the FFN is  $4d'$ . For training, a learning rate of 0.0001 is used, and we train the neural networks for 50000 iterations with the AdamW optimizer [24]. Meanwhile, as a common practice of deep generative models, we keep an exponential moving average (EMA) version of the model weights, and we always use the EMA weights for sampling [10]. This can be seen as an extra measure to stabilize the training. In terms of diffusion, we use  $S = 1000$  diffusion steps and accelerate the sampling using DPM-Solver [25] with 100 steps. A cosine noise schedule is adopted as in [16]. We only perform minimum preprocessing on the data, i.e., all data are linearly scaled to  $[-1, 1]$  using the minimum and the maximum values. We use 10-component GMM and t-Copula model [2] as our baselines. We selected these two baselines for their strengths in our evaluation metrics. GMM approximates the data's means and covariances, yielding low GFD and MMD scores. In contrast, t-Copula leverages the ECDF of the data, resulting in strong KL, WD, and KS scores.

## V. RESULTS

### A. Customer Level Evaluation

1) *Heat Pump Consumption*: For heat pump data of 1-minute to 1-hour resolutions, the 1-minute case is the most challenging in terms of GFD, as shown in Table II. All three models, *EnergyDiff*, GMM, and t-Copula, can achieve  $1 \times 10^{-3}$  level of GFD at 1 hour, but this number increases significantly to the level of  $1 \times 10$  at 1 minute. *EnergyDiff* shows superiority at the 1-minute resolution, with a 24.2% drop in GFD. *EnergyDiff* and GMM achieve the best and similar performance in terms of MMD. For marginal distribution-based metrics, KL, WD, and KS, t-Copula shows the best

TABLE II  
EVALUATION METRIC RESULTS ON WPUQ. BEST RESULTS ARE UNDERLINED.

Model	Res.	MMD	GFD	KL	WD	KS
GMM	1min	0.0009	12.5983	1.1547	0.0570	0.3109
t-Copula		0.0090	14.0475	<u>0.0029</u>	0.1048	<u>0.0998</u>
<i>E.Diff.</i>		<u>0.0007</u>	<u>9.5490</u>	0.2125	<u>0.0097</u>	0.2620
GMM	15min	<u>0.0008</u>	0.1145	0.3388	0.0261	0.1567
t-Copula		0.0024	0.1126	<u>0.0023</u>	<u>0.0017</u>	<u>0.0552</u>
<i>E.Diff.</i>		0.0009	<u>0.0087</u>	0.1494	0.0122	0.1315
GMM	30min	<u>0.0008</u>	0.0234	0.0943	0.0165	0.0991
t-Copula		0.0026	0.0281	<u>0.0030</u>	<u>0.0026</u>	<u>0.0322</u>
<i>E.Diff.</i>		<u>0.0008</u>	<u>0.0196</u>	0.0734	0.0086	0.0673
GMM	1h	0.0009	<u>0.0039</u>	0.0353	0.0094	0.0547
t-Copula		0.0015	0.0043	<u>0.0039</u>	<u>0.0035</u>	<u>0.0143</u>
<i>E.Diff.</i>		<u>0.0008</u>	0.0047	0.0255	0.0067	0.0410

*E.Diff.*: the proposed *EnergyDiff* framework.

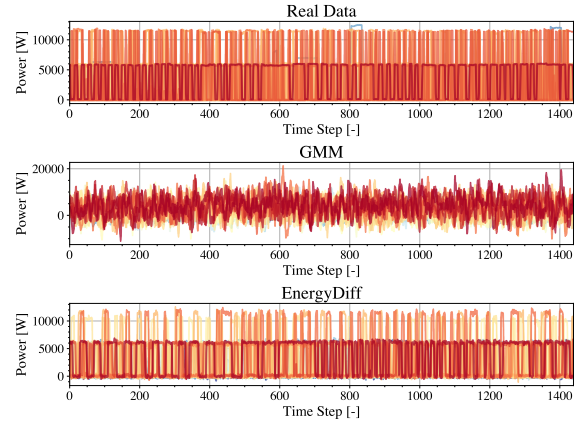


Fig. 4. WPUQ heat pump consumption curves at 1-minute resolution. Our model captures the periodical square wave-like pattern while GMM does not.

results in KL and KS, while *EnergyDiff* achieves the best in WD. GMM failed to obtain a decent KL score. Overall, at the 1-minute resolution, *EnergyDiff* demonstrates the best GFD and MMD with the best WD score, marking its excellent capability to learn both the temporal dependency and marginal distributions. While t-Copula and GMM have t-Copula or GMM require lower computational costs for the 1-hour or coarser resolutions, they necessitate a meticulous model selection process for each resolution. In contrast, our proposed *EnergyDiff* can be used universally across all resolutions, eliminating the need to develop separate models for each different time resolution.

We present randomly selected 100 real and generated heat pump consumption data samples in Fig. 4, corresponding to the numerical results in Table II. Despite the MMD between GMM and *EnergyDiff* being similar, we can observe in Fig. 4 that the synthetic samples of GMM are clearly unrealistic, as they do not contain the periodical temporal patterns of the real data. Meanwhile, the value range (minimum and maximum power) is incorrectly captured by GMM. While the real data has a maximum of around 10 kW and a minimum of 0 W, GMM produces unrealistic peaks of over 20 kW and negative values below  $-10$  kW. On the other hand, *EnergyDiff* successfully captures both the periodicity pattern and the value range.

Furthermore, in Fig. 5, we present the histograms of the same heat pump consumption data at the 1-minute resolution.

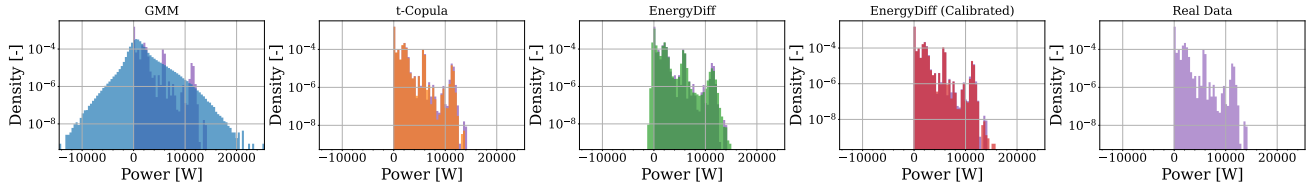


Fig. 5. Histograms of WPuQ heat pump consumption at 1 minute resolution. GMM fails to find the correct range of data. t-Copula fits exactly the empirical CDF. The proposed *EnergyDiff* fits the smoothed CDF, while after calibration, *EnergyDiff* fits the CDF perfectly.

TABLE III  
EVALUATION METRIC RESULTS ON LCL RESIDENTIAL ELECTRICITY LOAD PROFILES

Model	Res.	MMD	GFD	KL	WD	KS
GMM	30min	0.0015	<u>0.0096</u>	0.0499	0.0079	0.1117
t-Copula		0.0031	0.0170	0.0325	0.0038	<u>0.0938</u>
<i>E.Diff.</i>		<u>0.0014</u>	0.0134	<u>0.0043</u>	<u>0.0019</u>	0.1007
GMM	1h	<u>0.0014</u>	<u>0.0148</u>	0.0547	0.0082	0.1117
t-Copula		0.0033	0.0243	0.0315	0.0040	<u>0.0917</u>
<i>E.Diff.</i>		0.0016	0.0181	<u>0.0047</u>	<u>0.0027</u>	0.1118

TABLE IV  
EVALUATION METRIC RESULTS ON COSSMIC RESIDENTIAL ELECTRICITY LOAD PROFILES

Model	Res.	MMD	GFD	KL	WD	KS
GMM	1min	0.0026	2.8779	0.7455	0.0297	0.2090
t-Copula		***	***	***	***	***
<i>E.Diff.</i>		<u>0.0020</u>	<u>0.2642</u>	<u>0.5498</u>	<u>0.0102</u>	<u>0.1755</u>

\*\*\* indicates the model did not converge.

TABLE V  
EVALUATION METRIC RESULTS ON COSSMIC RESIDENTIAL PV GENERATION

Model	Res.	MMD	GFD	KL	WD	KS
GMM	1min	<u>0.0041</u>	6.6051	<u>0.0663</u>	0.0072	0.2284
t-Copula		***	***	***	***	***
<i>E.Diff.</i>		0.0042	<u>5.7764</u>	0.1684	<u>0.0064</u>	<u>0.2204</u>
GMM	15min	<u>0.0042</u>	<u>0.0001</u>	0.3239	<u>0.0006</u>	0.2287
t-Copula		***	***	***	***	***
<i>E.Diff.</i>		0.0382	0.0017	<u>0.0632</u>	0.0015	<u>0.1198</u>
GMM	30min	<u>0.0040</u>	<u>0.0002</u>	0.2050	<u>0.0008</u>	0.2175
t-Copula		***	***	***	***	***
<i>E.Diff.</i>		0.0117	0.0008	<u>0.0749</u>	0.0016	<u>0.1360</u>
GMM	1h	<u>0.0048</u>	<u>0.0003</u>	0.1898	<u>0.0010</u>	0.2067
t-Copula		***	***	***	***	***
<i>E.Diff.</i>		0.0076	0.0007	<u>0.0978</u>	0.0023	<u>0.1534</u>

To get the histogram, we count the consumption power of all time steps. The t-Copula model closely matches the histogram because it is designed to do so. *EnergyDiff* without calibration can capture the general pattern of the histogram but appears more smoothed, while the calibrated data matches the histogram exactly. In contrast, the GMM model fails to capture the distribution, as it struggles to find the correct support for the distribution and fails to capture the different modes of distribution.

2) *Residential Electricity Load Profile*: We evaluate *EnergyDiff*'s capability to model electricity load profile data on two datasets, LCL at 30-minute and 1-hour resolutions and CoSSMic at 1-minute resolutions. For the LCL dataset, as shown in Table III, our model and GMM achieve similarly good results in MMD and GFD at both time resolutions, while t-Copula performs worse. Although GMM's scores are slightly better than ours, the margin is small. Our model achieves the best results in KL and WD, whereas t-Copula achieves slightly better KS. Turning to the CoSSMic Dataset, our model delivers superior results across all metrics, demonstrating a significant improvement in GFD, reducing it from 2.8779 with GMM to 0.2642. For this dataset, t-Copula failed to converge during the fitting process. As evidenced by the numerical results on these two datasets, *EnergyDiff* demonstrate strong performance in generating residential electricity load profiles across various time resolutions.

3) *Residential PV Generation*: In Table V, we show the numerical results of the CoSSMic residential PV generation time series data. The t-Copula model failed to converge. Therefore, we only compare GMM and our model. At the 1-minute resolution, our model achieved the best results in three out of the five metrics: GFD, WD, and KS. The differ-

ence with GMM regarding MMD is only 0.0001, while the improvement in GFD is from 5.7764 to 6.6051. However, at 15-minute and 30-minute resolution, our model shows much worse performance in terms of MMD. This is likely due to this dataset's small sample size, as only 408 samples are available for training and 416 samples for evaluation. This suggests that *EnergyDiff* does not exhibit significant superiority at the 15-minute resolution and 30-minute resolution when the training set size is around or lower than 400 and the time resolution is 15 minutes or longer. This disadvantage can be compensated by pre-training *EnergyDiff* on a larger similar dataset and fine-tuning on the target dataset, as is done by other generative model research such as [12]. Our model's strong performance at the 1-minute resolution is likely due to its ability to capture the complex temporal dependencies in long time series data, a capability that GMM lacks.

## B. Transformer Level Evaluation

Our model can generate high-resolution energy time series data not only at the customer level but also at the transformer level. We present our experiment results in the WPuQ transformer electricity consumption dataset and the WPuQ transformer PV generation dataset. For simplicity, we only tested at the 1-minute resolution, as it is the most challenging case. Both datasets have over 1500 samples for training and evaluation. Tables VI and VII summarize the numerical results on these two datasets.

1) *Residential Electricity Load Profile*: In the WPuQ transformer case, the proposed *EnergyDiff* exhibits superior performance in terms of all five metrics, as shown in Table VI. Our model achieves 26.09% lower MMD and 11.65% lower GFD than GMM, suggesting our generated data have a more similar temporal dependency with the real data.

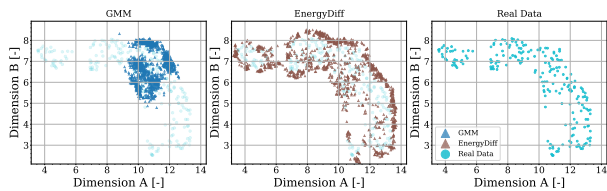


Fig. 6. UMAP visualization of WPUQ transformer measurement data. Our model captures the complete manifold of the real data, while GMM fails to do so.

TABLE VI  
EVALUATION METRIC RESULTS ON WPUQ TRANSFORMER-LEVEL RESIDENTIAL ELECTRICITY LOAD PROFILES

Model	Res.	MMD	GFD	KL	WD	KS
GMM		0.0092	12.2992	0.0125	0.0231	0.0500
t-Copula	1min	***	***	***	***	***
<i>E.Diff.</i>		<u>0.0068</u>	<u>10.8667</u>	<u>0.0072</u>	<u>0.0129</u>	<u>0.0263</u>

Visualizing the temporal patterns of a 1440-step time series is difficult in general. Therefore, to better understand these high-dimensional time series, we use a dimensionality reduction tool, UMAP [26], to reduce the data into 2-dimensional. UMAP learns a manifold of the high-dimensional data and re-maps the manifold into the 2D space. As in Fig. 6, the data generated by *EnergyDiff* covers the whole manifold of the real data. Meanwhile, the figure demonstrates that our model does not merely replicate the training data points but instead interpolates and extrapolates data that align with the real manifold. However, data generated by GMM span only part of the manifold, indicating a discrepancy between GMM and the real data distribution. This suggests that using GMM synthetic data for energy system operation and planning could over-represent some scenarios and under-represent others, potentially leading to sub-optimal decisions.

2) *Residential PV Generation*: We show the numerical results for the WPUQ transformer PV generation dataset in Table VII. We observe that *EnergyDiff* and GMM achieve very similar performance across all metrics. To further assess whether the synthetic data of both models are of similar quality, we visualize 100 real and synthetic samples from these two models in Fig. 7. It is noticed that both models capture the coarse wave shape of the data, i.e., zero generation during night time and peak generation around noon. However, GMM again shows unrealistic negative values. Meanwhile, most of the peak values of the real data lie around 15kW, while the peak values of GMM data are overestimated.

### C. Marginal Calibration Evaluation

Next, we demonstrate the effect of the proposed Marginal Calibration. As an example, we pick the WPUQ heat pump dataset at the 1-minute resolution. We compare the numerical evaluation metrics before and after calibration in Table VIII. We noticed that the MMD and GFD scores have slightly degraded but are still competitive, while KL, WD, and KS have improved significantly and have surpassed t-Copula.

Furthermore, we randomly select two consecutive time steps to visualize the temporal pattern differences in Fig. 8. Here, we have selected the 115-th and 116-th time steps, corresponding to 01:55 and 01:56 midnight. We observe

TABLE VII  
EVALUATION METRIC RESULTS ON WPUQ TRANSFORMER-LEVEL PV GENERATION

Model	Res.	MMD	GFD	KL	WD	KS
GMM		<u>0.0010</u>	<u>3.4678</u>	<u>0.0260</u>	0.0192	0.2733
t-Copula	1min	***	***	***	***	***
<i>E.Diff.</i>		0.0011	3.8651	0.0471	<u>0.0062</u>	<u>0.2287</u>

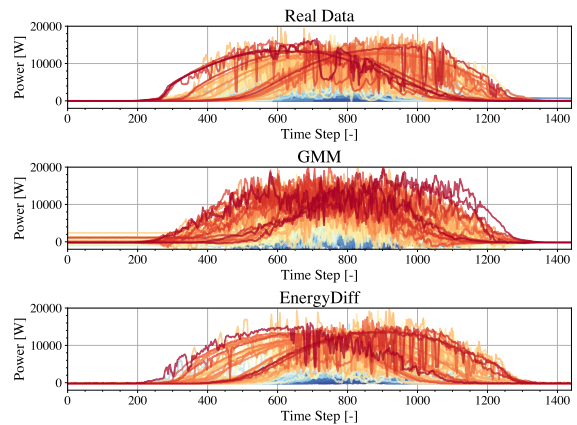


Fig. 7. WPUQ PV generation curves in 1 minute resolution. GMM samples are overly noisy and contain unrealistic negative values.

small changes in the scatter plot in the middle. However, the marginal distributions are brought closer to the real data. This is because our calibration is based on OT, which minimizes the changes but guarantees the calibrated data has the exact CDF of the training data. The remaining mismatch of the marginal distributions is due to the ECDF estimation error from the training data. However, this mismatch is small, proven by the numerical results in Table VIII.

### D. Computation Time and Stability

The training time of GMM, t-Copula, and *EnergyDiff* varies significantly. *EnergyDiff* requires approximately 3 hours for 1-minute resolution data and 1 hour for 1-hour resolution data. Generating 4000 instances of 1-minute data from *EnergyDiff* takes around 8 minutes, while it only takes seconds for 1-hour data. The GMM is more computation-efficient, with both fitting and sampling taking less than 1 minute. Fitting the t-Copula model for the 1-minute resolution takes approximately 15 minutes but frequently fails due to the numerical instability of the optimization process. Notably, in several datasets like the CoSSMic residential electricity load profile, t-Copula failed to converge despite multiple tries. We observe that this instability is particularly exacerbated in high-resolution data, such as 1 minute, and when the training set size is thousands or larger. Overall, *EnergyDiff* and GMM are computationally robust, while GMM is the most computation-efficient model.

## VI. CONCLUSION

DDPMs are powerful generative models that have become the most popular choice in the image and audio generation domain. However, the standard DDPM has high computation and memory complexity related to the input data size, making them unsuitable for generating high-resolution time series data

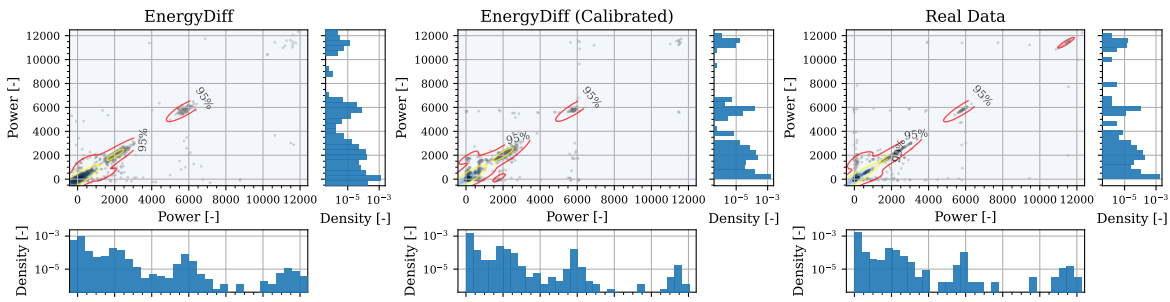


Fig. 8. **Top left** is a scatter plot of the real and generated heat pump data by *EnergyDiff* at the 115-th and 116-th step, before and after the marginal calibration. Gray dots are data points. Contour lines are based on Gaussian kernel density estimation. **Bottom** and **Top right** are the corresponding marginal distributions. The proposed calibration applies the minimum change to the data but makes the marginal distributions almost exactly match the real data.

TABLE VIII  
MARGINAL CALIBRATION COMPARISON ON WPUQ HEAT PUMP CONSUMPTION

Model	MMD	GFD	KL	WD	KS
GMM	0.0009	12.5983	1.1547	0.0570	0.3109
t-Copula	0.0090	14.0475	0.0029	0.1048	0.0998
<i>E.Diff.</i> w/o*	0.0007	9.5490	0.2125	0.0097	0.2620
<i>E.Diff.</i> w/**	0.0032	10.5731	0.0018	0.0023	0.0129

w/o\* without Marginal Calibration  
w/\*\* with Marginal Calibration

such as 1440-step 1-minute daily load profiles. Additionally, despite their capability to capture complex dependencies, they do not necessarily yield precise marginal distributions, which is crucial for accurately representing high-consumption or high-generation scenarios. To address these issues, we proposed *EnergyDiff*, a DDPM-based universal energy time series generation framework. With a tailored denoising process, *EnergyDiff* generates high-quality data across different energy domains at various time resolutions and both the customer and transformer levels. Our proposed Marginal Calibration technique ensures that *EnergyDiff* captures precise marginal distributions.

## REFERENCES

- [1] K. Vemalaiah, D. K. Khatod, and N. P. Padhy, “Synergistic day-ahead scheduling framework for smart distribution grid under uncertainty,” *IEEE Trans. Ind. Inf.*, vol. 20, no. 7, pp. 9681–9691, Jul. 2024.
- [2] E. M. S. Duque, P. P. Vergara, P. H. Nguyen, A. van der Molen, and J. G. Slootweg, “Conditional Multivariate Elliptical Copulas to Model Residential Load Profiles From Smart Meter Data,” *IEEE Trans. Smart Grid*, vol. 12, no. 5, pp. 4280–4294, Sep. 2021.
- [3] Y. Sun, A. Cuesta-Infante, and K. Veeramachaneni, “Learning Vine Copula Models for Synthetic Data Generation,” *Proc. AAAI Conf. Artif. Intell.*, vol. 33, no. 01, pp. 5049–5057, Jul. 2019.
- [4] L. Song, Y. Li, and N. Lu, “ProfileSR-GAN: A GAN Based Super-Resolution Method for Generating High-Resolution Load Profiles,” *IEEE Trans. Smart Grid*, vol. 13, no. 4, pp. 3278–3289, Jul. 2022.
- [5] Z. Ma, G. Mei, and F. Piccialli, “An attention-based cycle-consistent generative adversarial network for IoT data generation and its application in smart energy systems,” *IEEE Trans. Ind. Inf.*, vol. 19, no. 4, pp. 6170–6181, Apr. 2023.
- [6] Z. Pan, J. Wang, W. Liao, H. Chen, D. Yuan, W. Zhu, X. Fang, and Z. Zhu, “Data-Driven EV Load Profiles Generation Using a Variational Auto-Encoder,” *Energies*, vol. 12, no. 5, p. 849, Jan. 2019.
- [7] W. Xia, C. Wang, P. Palensky, and P. P. Vergara, “A flow-based model for conditional and probabilistic electricity consumption profile generation and prediction,” May 2024.
- [8] I. J. Goodfellow, J. Pouget-Abadie, M. Mirza, B. Xu, D. Warde-Farley, S. Ozair, A. Courville, and Y. Bengio, “Generative Adversarial Networks,” *arXiv:1406.2661 [cs stat]*, Jun. 2014.

- [9] M. Arjovsky and L. Bottou, “Towards principled methods for training generative adversarial networks,” Jan. 2017.
- [10] J. Ho, A. Jain, and P. Abbeel, “Denoising diffusion probabilistic models,” in *Advances in Neural Information Processing Systems*, vol. 33. Curran Associates, Inc., 2020, pp. 6840–6851.
- [11] P. Dhariwal and A. Nichol, “Diffusion Models Beat GANs on Image Synthesis,” in *Advances in Neural Information Processing Systems*, vol. 34. Curran Associates, Inc., 2021, pp. 8780–8794.
- [12] W. Peebles and S. Xie, “Scalable diffusion models with transformers,” in *Proceedings of the IEEE/CVF International Conference on Computer Vision*, 2023, pp. 4195–4205.
- [13] A. Vaswani, N. Shazeer, N. Parmar, J. Uszkoreit, L. Jones, A. N. Gomez, E. Kaiser, and I. Polosukhin, “Attention is All you Need,” in *Advances in Neural Information Processing Systems*, vol. 30. Curran Associates, Inc., 2017.
- [14] S. Li, H. Xiong, and Y. Chen, “DiffCharge: Generating EV Charging Scenarios via a Denoising Diffusion Model,” *IEEE Transactions on Smart Grid*, pp. 1–1, 2024.
- [15] J. Li, Z. Chen, L. Cheng, and X. Liu, “Energy data generation with Wasserstein Deep Convolutional Generative Adversarial Networks,” *Energy*, vol. 257, p. 124694, Oct. 2022.
- [16] A. Q. Nichol and P. Dhariwal, “Improved denoising diffusion probabilistic models,” in *International Conference on Machine Learning*. PMLR, Jul. 2021, pp. 8162–8171.
- [17] D. Hendrycks and K. Gimpel, “Gaussian error linear units (GELUs),” Jun. 2023.
- [18] X. Ding, X. Zhang, J. Han, and G. Ding, “Scaling up your kernels to 31x31: Revisiting large kernel design in CNNs,” in *Proceedings of the IEEE/CVF Conference on Computer Vision and Pattern Recognition*, 2022, pp. 11 963–11 975.
- [19] E. Carpaneto and G. Chicco, “Probabilistic characterisation of the aggregated residential load patterns,” *IET Gener. Transm. amp; Distrib.*, vol. 2, no. 3, pp. 373–382, May 2008.
- [20] J. Schofield, S. Tindemans, R. Carmichael, M. Woolf, M. Bilton, and G. Strbac, “Low carbon london project: Data from the dynamic time-of-use electricity pricing trial, 2013,” Jan. 2016.
- [21] M. Schlemminger, T. Ohrdes, E. Schneider, and M. Knoop, “Dataset on electrical single-family house and heat pump load profiles in Germany,” *Sci. Data*, vol. 9, no. 1, p. 56, Feb. 2022.
- [22] A. Amato, B. Di Martino, M. Scialdone, and S. Venticinque, “Towards a SLA for collaborating smart solar-powered micro-grids,” in *2014 International Conference on Intelligent Networking and Collaborative Systems*, Sep. 2014, pp. 592–597.
- [23] W. Xia, H. Huang, E. M. S. Duque, S. Hou, P. Palensky, and P. P. Vergara, “Comparative assessment of generative models for transformer- and consumer-level load profiles generation,” *Sustainable Energy Grids Networks*, vol. 38, p. 101338, Jun. 2024.
- [24] I. Loshchilov and F. Hutter, “Decoupled weight decay regularization,” Jan. 2019.
- [25] C. Lu, Y. Zhou, F. Bao, J. Chen, C. Li, and J. Zhu, “DPM-Solver: A Fast ODE Solver for Diffusion Probabilistic Model Sampling in Around 10 Steps,” in *Advances in Neural Information Processing Systems*, May 2022.
- [26] L. McInnes, J. Healy, and J. Melville, “UMAP: Uniform Manifold Approximation and Projection for Dimension Reduction,” Sep. 2020.